Published in final edited form as:
J Biomech. 2010 August 26; 43(12): 2315–2320. doi:10.1016/j.jbiomech.2010.04.031.

Quantitative, Structural and Image-based Mechanical Analysis of Nonunion Fracture Repaired by Genetically Engineered Mesenchymal Stem Cells

Ilan Kallai[a,*], **G. Harry van Lenthe**[b,c,*], **Davide Ruffoni**[b], **Yoram Zilberman**[a], **Ralph Müller**[b], **Gadi Pelled**[a,d], and **Dan Gazit**[a,d]

[a]Skeletal Biotech Laboratory, Hebrew University–Hadassah Faculty of Dental Medicine, Ein Kerem Jerusalem, Israel [b]Institute for Biomechanics, ETH Zurich, Zurich, Switzerland [c]Division of Biomechanics, K.U.Leuven, Leuven, Belgium [d]Department of Surgery and Cedars-Sinai Regenerative Medicine Institute (CS-RMI), Cedars Sinai Medical Center, Los Angeles, CA, USA

Abstract

Stem cell-mediated gene therapy for fracture repair, utilizes genetically engineered mesenchymal stem cells (MSCs) for the induction of bone growth and is considered a promising approach in skeletal tissue regeneration. Previous studies have shown that murine nonunion fractures can be repaired by implanting MSCs over-expressing recombinant human bone morphogenetic protein-2 (rhBMP-2). Nanoindentation studies of bone tissue induced by MSCs in a radius fracture site indicated similar elastic modulus compared to intact murine bone, eight weeks post treatment. In the present study we sought to investigate temporal changes in microarchitecture and biomechanical properties of repaired murine radius bones, following the implantation of MSCs. High resolution micro computed tomography (Micro-CT) was performed 10 and 35 weeks post MSC implantation, followed by micro finite element (Micro-FE) analysis. The results have shown that the regenerated bone tissue remodels over time, as indicated by a significant decrease in bone volume, total volume and connectivity density combined with an increase in mineral density. In addition, the axial stiffness of limbs repaired with MSCs was 2 to 1.5 times higher compared to the contralateral intact limbs, at 10 and 35 weeks post treatment. These results could be attributed to the fusion that occurred between in the ulna and radius bones. In conclusion, although MSCs induce bone formation, which exceeds the fracture site, significant remodeling of the repair callus occurs over time. In addition, limbs treated with an MSC graft demonstrated superior biomechanical properties, which could indicate the clinical benefit of future MSC application in nonunion fracture repair.

Keywords

Micro finite element model; Micro computed tomography; Bone tissue regeneration; Mesenchymal stem cells

Corresponding author: Dan Gazit, Skeletal Biotechnology Laboratory, Hebrew University- Hadassah Medical Campus, PO BOX 12272, Ein Kerem, Jerusalem 91120, Israel, Lab Tel: 972-2-6757627, Fax: 972-2-6757628, dgaz@cc.huji.ac.il.
*Both authors equally contributed to this manuscript

Introduction

Although bone tissue has regenerative capabilities, in extreme situations in which the extent of bone loss or damage due to trauma, surgery, or a metabolic disease such as osteoporosis is too large, complete regeneration will not occur. Therefore, the induction of *in vivo* bone formation is a major goal in a variety of orthopedic and neurosurgical procedures, such as segmental bone fractures and spinal fusion.

Mesenchymal stem cells (MSCs) reside in bone marrow and can also be isolated from other adult tissues like adipose (Sheyn et al., 2008). We have previously shown that, MSCs, genetically engineered to over-express a bone morphogenetic protein (BMP) gene, can be utilized to achieve accelerated bone regeneration in a segmental fracture (Gazit et al., 1999; Turgeman et al., 2001) and spine fusion models (Hasharoni et al., 2005; Sheyn et al., 2008). These genetically engineered MSCs have an enhanced therapeutic effect in healing bone segmental defects due to a dual mechanism: a paracrine mechanism by which rhBMP-2 exerts its osteoinductive effects on host cells, and an autocrine mechanism in which rhBMP-2 induces the osteogenic differentiation of the transplanted genetically-engineered stem cells (Gazit et al., 1999). Indeed our studies showed that prominent bone tissue was generated at the site of genetically engineered MSC implantation, often exceeding the boundaries of the fracture site, in a manner similar to callus formation. Yet, it was unknown whether the repair bone generated by the implanted MSCs remodels in the same way a fracture callus does.

Micro–computed tomography (Micro-CT) is an X-ray–based microstructural imaging method that allows an easy and relatively inexpensive access to the 3-D microarchitecture of bone, thereby providing a powerful tool for the exploration of bone regeneration. In a recent study (Morgan et al., 2009), an extensive analysis was performed on 188 murine fracture calluses at multiple time points and under varying experimental conditions. Importantly, it was found that micro-CT-based measures of callus structure were able to provide good prediction of fracture callus' mechanical properties.

Indeed, one of the major outcome measures of bone regeneration is the biomechanical property of the repaired tissue. Where micro-CT measures can be useful in a non-invasive evaluation of fracture callus' mechanical competence, they only do so in a statistical sense. They cannot be relied on to explain the real physical contribution of the microarchitecture to bone competence. To understand how differences in bone microarchitecture influence bone stiffness and strength, insight into load transfer through bone architecture is needed. Such information could come from experimental biomechanical tests and from microstructural finite element (micro-FE) models. Although experimental biomechanical tests are considered the gold standard to determine mechanical competence, state-of-the-art micro-FE models generated directly from computer reconstructions of bone structure allow performing virtual biomechanical tests that resemble experimental biomechanical tests in great detail and with high precision. These computer models allow calculation of loads at the microstructural or even the tissue level (van Rietbergen et al., 1995; Ladd et al., 1998) and have been used extensively to determine accurately the apparent mechanical properties of bone specimens. It has also been used to quantify fracture callus mechanical properties (Shefelbine et al., 2005); in that study FE-predicted callus rigidity correlated significantly better with experimental torsional rigidity than other common measures of healing. It is true that FE analysis is subject to several assumptions and simplifications. Nevertheless, excellent agreement has been found in several studies between computationally derived stiffness and experimentally measured stiffness, such that FE is considered validated for the assessment of apparent stiffness in linear-elastic analyses (Ladd et al., 1998; Kabel et al., 1999; Homminga et al., 2003).

In this study we used rhBMP-2 over-expressing MSCs to induce nonunion fracture repair in a murine model. We have previously utilized ex-vivo nanobiomechanics in order to analyze the intrinsic mechanical properties of new bone formed by engineered MSCs in a similar model (Tai et al., 2008). Our results showed that intact radius bone exhibited a statistically similar elastic modulus values compared to that of the regenerated bone, while the hardness was found to be marginally statistically different at 1000 μN and statistically similar at 7000 μN. However, that study did not investigate the biomechanical properties of the entire repaired limb. Therefore, our aim in this study was to analyze bone stiffness using micro-FE and combining it with micro-CT analyses of bone formation to obtain a better understanding of the quality of nonunion fracture repair by engineered MSC implantation. In addition, we investigated the natural remodeling changes that occur in the regenerated bone over time, utilizing structural analysis based on the micro-CT scans.

Materials and Methods

Genetically engineered mesenchymal stem cells with controllable expression of rhBMP-2

RhBMP-2 over-expressing MSCs, a C3H10T1/2-derived stem cell line genetically engineered to express the rhBMP-2 gene under tetracycline-off regulation, was generated as previously described (Moutsatsos et al., 2001). Cells were cultured in Dulbecco's modified Eagle medium with 4.5 g/L D-glucose (Biological Industries, Beit-Haemek, Israel) containing 10% fetal calf serum (Biological Industries),100 U/ml penicillin–streptomycin (Biological Industries), 2 mM L-glutamine (Biological Industries), and 1 mg/ml doxycycline (Sigma–Aldrich, St. Louis, MO, USA) to prevent the expression of rhBMP-2 during the culture period.

Animals Preparation

For this study we used 24 C3H/HeN female mice ranging from 6 to 8 weeks of age. C3H/HeN mice (Harlan, Israel), from which C3H10T1/2 cells had been originated, were selected in order to avoid an immune reaction against the implanted cells. The Institutional Animal Care and Use Committee of the Hebrew University approved all the procedures used in this study. All animals were provided free access to food and water throughout the entire study.

Anesthesia was induced in each mouse by an intraperitoneal injection of ketamine–xylazine solution (1 μl/g body weight). For analgesia and an anti-inflammatory effect, each animal was also given an intraperitoneal injection of Rimadyl (5 mg/ml). Fur covering the right fore limb of the animal was shaved using an electric hair shaver, and the skin was prepared by rubbing it with a swab that had been dipped in isopropanol (70%) and chlorhexidine (0.1%).

In vivo cell implantations

A 2.5-mm nonunion defect was created in the radius bone of each mouse in the experimental group, as we have previously described (Gazit et al., 1999; Moutsatsos et al., 2001). In brief, after anesthesia and surgical preparation, skin was cut in the middle of the right forelimb, muscles bluntly dissected and exposed radius. 2.5 mm of the exposed radius were cut using a bone cutter. The dissected 2.5 mm bone fragment was removed, creating a nonunion bone defect. Then 2×10^6 genetically engineered MSCs were trypsinized, suspended in 30 μl PBS, loaded onto a standard 1 × 3–mm collagen sponge (DuraGen; Integra LifeSciences Corporation, NJ, USA) and implanted into the bone defect (Fig. 1a). In addition, a non-resorbable Teflon sheet was inserted between the radius and ulna. The contralateral limbs of the same mice, which were not subjected to surgery, were used as controls.

Micro-CT evaluation of bone formation

Bone formation in nonunion fractures, was evaluated using micro-CT as we have previously described (Zilberman et al., 2008). 10 weeks after implantation, 12 mice were killed and the mouse forelimbs (including the ulna and radius) as well as intact muscle and soft tissue were measured using a Desktop Cone-Beam Micro-CT Scanner (μCT 40; Scanco Medical AG, Bassersdorf, Switzerland). 35 weeks after implantation, the other 12 mice were killed and the forelimbs were measured. Micro-tomographic slices were acquired at 1000 projections and reconstructed at a spatial nominal resolution of 20μm. A constrained 3-D Gaussian filter ($\sigma = 0.8$ and support = 1) was used to partly suppress the noise in the volumes. The bone tissue was segmented from marrow and soft tissue by using a global thresholding procedure (Müller and Ruegsegger, 1997). In addition to the visual assessment of structural images, morphometric indices were determined from the microtomographic data sets by using direct 3-D morphometry (Hildebrand et al., 1999). In the nonunion fracture site, we only evaluated the central 2 mm of the bone defect (of total 2.5 mm), which included only newly formed bone. Our evaluation of the non fractured control bone also focused on the central 2 mm of the radius. Structural metrics measured using micro-CT are closely correlated with those measured using standard histomorphometry (Müller et al., 1998). The following morphometric indices were determined: (i) total volume of bone (TV, mm^3), including new bone and soft tissue cavities; (ii) volume of mineralized bone tissue (BV, mm^3); (iii) bone volume density, (BV/TV, -); (iv) connectivity density (Conn.Dens, $1/mm^3$), describing the porosity of the bone sample and shows how branched is the bone tissue structure; (v) average bone thickness (B.Th, mm), calculated as average thickness of all bone voxels, defined as Tb.Th* by Hildebrand et al. (1999); (vi) average bone separation, the thickness of cavities (B.Sp, mm), defined as Tb.Sp* by Hildebrand et al. (1999); (vii) bone mineral density (BMD, mg hydroxyapatite /cm^3) derived from the projectional image and calculated based on calibration with commercially available Micro-CT phantom containing H_2KPO_4 (Scanco Medical AG, Bassersdorf, Switzerland); and (viii) degree of anisotropy (DA).

Micro-FE analysis

We created micro-FE models of the middle 8 mm of the radius bones by using a direct voxel conversion technique; each voxel from the micro-CT reconstruction was converted to a hexahedral element in the micro-FE model. Before conversion, all 3D reconstructions were automatically oriented so that their final orientation was similar. For that purpose, the middle 75% of the radius was selected and rotated such that the main axes of the inertia tensor were parallel to the global reference system. The models included the ulna because that bone had adapted as well; furthermore, the radius and ulna were often tightly connected. Component labeling was performed to assure that no loose bone fragments were included in the FE models. Boundary conditions were applied that represented an axial compression test; the distal part of the each model was fully fixed, whereas the proximal part underwent an axial displacement, resulting in 1% overall strain. A scheme of the micro-FE model is shown in figure 1c. The regenerated and intact bones were modeled with an isotropic tissue modulus of 13.4 GPa (van Lenthe et al., 2008). All elements were assigned a Poisson ratio of 0.3. Assuming linear-elastic behavior, the models were solved using the dedicated linear finite element package ParFE (Arbenz et al., 2008). The models were used to calculate the force needed to obtain the prescribed displacement, from which apparent stiffness was derived.

Histological evaluation

After the ex-vivo micro-CT measurements, samples of forelimb implanted with MSCs were fixed in 4% formalin, decalcified in the histological decalcifying agent Calci-Clear Rapid (National Diagnostics, Atlanta, GA), dehydrated, embedded in paraffin, cut into 5-μm thick sections, and stained using hematoxylin and eosin (H&E).

Statistical analysis

For all structural indices and bone stiffness data, two-tailed homoscedastic student's t-tests were conducted using Microsoft Excel software (Microsoft Corporation, Redmond, WA, USA).

Results

Micro-CT analysis

Prominent new bone tissue formation was detected in the nonunion fracture sites. The regenerated bone tissue (Fig. 2b-c) demonstrated different morphology compared to the intact control (Fig. 2a). The 2D images display changes in the regenerated bone morphology with time (Fig. 2b vs. c). These images highlight the powerful osteogenic potential of genetically engineered MSCs, which induce robust bone formation within a short period of time. One mouse of each group was omitted from the structural analysis because the healing was not complete. Quantitative analysis of the newly formed bone in the nonunion fracture site, at 10 vs. 35 weeks after implantation, showed a significant decrease in bone volume, total volume and connectivity density (Fig. 3a-c) and an increase in bone mineral density (Fig. 3d). The structural indices of the regenerated bones, at 35 weeks, were closer to the indices of the intact untreated bones, than the indices at 10 weeks. All structural indices that were derived are shown in Table 1 and 2 (included in the appendix).

Micro-FE analysis

The micro-FE analysis of the MSC-treated limb showed that the healed bones were substantially stronger than the control ones. When using a tissue modulus of 13.4 GPa, the stiffness (mean±SE) of the treated limb was 1035.5 ± 13.4 N/mm compared with 522.8 ± 14.0 N/mm of the intact limb (Fig. 4). The micro-FE analysis also showed that this new bone was not highly stressed (data not shown). This was probably due to an increased cross-sectional area of the fracture site in the treated radii, and due to a partial fusion of the radius and ulna (shown in Fig. 5); both effects resulted in an increase in cross-sectional moment of area, thereby stiffening the limb.

Discussion

MSC-mediated bone regeneration is a promising approach for the treatment of segmental bone fractures and other orthopaedic conditions in which bone formation is needed, such as spine fusion. Others and we have shown that MSCs overexpressing osteogenic genes such as BMP-2 induce accelerated fracture repair in non-union fracture models. Yet, it most cases excessive bone formation was evident at the implantation site (Lieberman et al., 1998; Gazit et al., 1999; Moutsatsos et al., 2001; Turgeman et al., 2001; Hsu et al., 2007; Tai et al., 2008; Zilberman et al., 2008). In addition, little is known of the biomechanical properties of fractured limbs repaired by genetically engineered MSCs. In the current study we hypothesized that the implantation of BMP-2 over-expressing MSCs in a nonunion bone defect would result in new bone regeneration, which would remodel over time and provid biomechanical competence to the treated limb. Indeed the results presented here showed that 10 weeks post implantation, the structural indices of the newly formed bone at the fracture site were significantly different ($p < 0.001$) from the intact contralateral radius bones, being composed of a larger mass of thin bone compartments with lower mineral density. At 35 weeks post treatment, the structural indices of the regenerated bones were significantly different than the indices at 10 weeks and closer to the indices of the intact untreated bones. In this study we have not evaluated bone regeneration using non-engineered MSCs or, collagen scaffolds only since our previous studies have shown that these treatments did not

result in bone formation and fracture repair (Gazit et al., 1999; Moutsatsos et al., 2001; Turgeman et al., 2001; Zilberman et al., 2008).

The relevance of micro-CT measures in assessing callus healing has been clearly demonstrated (Morgan et al., 2009). We used micro-CT-based FE models that have previously been validated for the mechanical evaluation of C3H murine bones (van Lenthe et al, 2008). In the present study, the micro-CT scans captured the mineralized bone fraction of the newly formed bone with great detail. As we used a direct voxel-to-element conversion, our micro-FE models also represented in detail these intricate structures, as well as their three-dimensional orientation and integration with the host bone; this allowed us to show that the bone formed by engineered MSCs had good structural integrity.

Torsional testing is a common experimental approach to quantify fracture callus mechanical competence. However, torsional testing becomes a non-trivial technique given the close interaction between radius and ulna, requiring the need to test both bones in one experiment. Hence, establishing a pure torsion test for the two bones in combination seems impossible, because of the inability to define the loading axis. Therefore, we simulated axial compression because it captured aspects of callus competence, but had the advantage that proper boundary conditions were readily defined. The axial stiffness of the limbs repaired with engineered MSCs was approximately two times higher than the stiffness of the contralateral intact limbs. Our results showed that the cause for the substantial increase in stiffness of the treated limbs could be found in the high degree of fusion between the radius and the ulna (demonstrated by the histological evaluation in Fig.5). On top of that, the ulna showed substantial remodeling, which could potentially add to the stiffening of the bones. Future studies using this fracture-healing model should include calculating the direction-dependence of elastic properties, in order to shed more light on the biomechanical properties of the regenerated bones.

It is known that newly formed bone tissue has lower stiffness values than mature bone (Miller et al., 2007). However, using nanoindentation we previously showed that after 8 weeks of treatment with BMP-2 over-expressing MSCs, the stiffness of a newly formed bone is similar to that of intact bone (Tai et al., 2008). Therefore in the present study we hypothesized that the tissue modulus of the newly formed bone after 10 and 35 weeks would be even more similar to that of intact bone.

The detailed physiological loading conditions at the radius are unknown. We simulated axial compression as a major component of normal loading. Due to the curvature of the radius and ulna this caused bending. Under normal physiological loading these bones will also be subject to bending moments. As the treated bones were already stiffer under axial compression, this will be even more so when loaded under pure bending because the cross-sectional moments of inertia of the treated bones were much higher than those for the control ones.

The most important feature of the methods used in this study was the nondestructive examination of the bones using micro-CT. Although this aspect did not have major influence on our study design, it provides us the possibility to design future studies in which we could measure the same parameters in the living animal over time. Other advantages of this type of analysis are that the complete geometric and structural organizations of a particular bone are taken into account and realistic boundary conditions to model the musculoskeletal interface can be applied. Future studies using in-vivo micro-CT imaging followed by mechanical analysis based on micro-FE should be validated with mechanical testing.

We conclude that the implantation of MSCs engineered to express the BMP-2 gene leads to nonunion fracture repair with biomechanically competent bone tissue. These results could be valuable for future applications of genetically engineered MSCs in the clinical setting.

Supplementary Material

Refer to Web version on PubMed Central for supplementary material.

Acknowledgments

We thank the Swiss National Supercomputing Centre (CSCS) for granting computational time.

We acknowledge funding from the National Institutes of Health Grants No. R01AR056694-01A1 and R01DE019902-01 (D.G. and G.P.).

References

Arbenz P, van Lenthe GH, Mennel U, Müller R, Sala M. A scalable multi-level preconditioner for matrix-free μ-finite element analysis of human bone structures. International Journal for Numerical Methods in Engineering. 2008; 73:927–947.

Gazit D, Turgeman G, Kelley P, Wang E, Jalenak M, Zilberman Y, Moutsatsos I. Engineered pluripotent mesenchymal cells integrate and differentiate in regenerating bone: A novel cell-mediated gene therapy. J Gene Med. 1999; 1:121–133. [PubMed: 10738576]

Hasharoni A, Zilberman Y, Turgeman G, Helm GA, Liebergall M, Gazit D. Murine spinal fusion induced by engineered mesenchymal stem cells that conditionally express bone morphogenetic protein-2. J Neurosurg Spine. 2005; 3:47–52. [PubMed: 16122022]

Hildebrand T, Laib A, Müller R, Dequeker J, Ruegsegger P. Direct three-dimensional morphometric analysis of human cancellous bone: Microstructural data from spine, femur, iliac crest, and calcaneus. J Bone Miner Res. 1999; 14:1167–1174. [PubMed: 10404017]

Homminga J, McCreadie BR, Weinans H, Huiskes R. The dependence of the elastic properties of osteoporotic cancellous bone on volume fraction and fabric. J Biomech. 2003; 36:1461–1467. [PubMed: 14499295]

Hsu WK, Sugiyama O, Park SH, Conduah A, Feeley BT, Liu NQ, Krenek L, Virk MS, An DS, Chen IS, Lieberman JR. Lentiviral-mediated bmp-2 gene transfer enhances healing of segmental femoral defects in rats. Bone. 2007; 40:931–938. [PubMed: 17236835]

Kabel J, van Rietbergen B, Dalstra M, Odgaard A, Huiskes R. The role of an effective isotropic tissue modulus in the elastic properties of cancellous bone. J Biomech. 1999; 32:673–680. [PubMed: 10400354]

Ladd AJ, Kinney JH, Haupt DL, Goldstein SA. Finite-element modeling of trabecular bone: Comparison with mechanical testing and determination of tissue modulus. J Orthop Res. 1998; 16:622–628. [PubMed: 9820288]

Lieberman JR, Le LQ, Wu L, Finerman GA, Berk A, Witte ON, Stevenson S. Regional gene therapy with a bmp-2-producing murine stromal cell line induces heterotopic and orthotopic bone formation in rodents. J Orthop Res. 1998; 16:330–339. [PubMed: 9671928]

Miller LM, Little W, Schirmer A, Sheik F, Busa B, Judex S. Accretion of bone quantity and quality in the developing mouse skeleton. J Bone Miner Res. 2007; 22:1037–1045. [PubMed: 17402847]

Morgan EF, Mason ZD, Chien KB, Pfeiffer AJ, Barnes GL, Einhorn TA, Gerstenfeld LC. Micro-computed tomography assessment of fracture healing: Relationships among callus structure, composition, and mechanical function. Bone. 2009; 44:335–344. [PubMed: 19013264]

Moutsatsos IK, Turgeman G, Zhou S, Kurkalli BG, Pelled G, Tzur L, Kelley P, Stumm N, Mi S, Müller R, Zilberman Y, Gazit D. Exogenously regulated stem cell-mediated gene therapy for bone regeneration. Molecular Therapy. 2001; 3:449–461. [PubMed: 11319905]

Müller R, Ruegsegger P. Micro-tomographic imaging for the nondestructive evaluation of trabecular bone architecture. Stud Health Technol Inform. 1997; 40:61–79. [PubMed: 10168883]

Müller R, Van Campenhout H, Van Damme B, Van Der Perre G, Dequeker J, Hildebrand T, Ruegsegger P. Morphometric analysis of human bone biopsies: A quantitative structural comparison of histological sections and micro-computed tomography. Bone. 1998; 23:59–66. [PubMed: 9662131]

Shefelbine SJ, Simon U, Claes L, Gold A, Gabet Y, Bab I, Müller R, Augat P. Prediction of fracture callus mechanical properties using micro-ct images and voxel-based finite element analysis. Bone. 2005

Sheyn D, Pelled G, Zilberman Y, Talasazan F, Frank JM, Gazit D, Gazit Z. Nonvirally engineered porcine adipose tissue-derived stem cells: Use in posterior spinal fusion. Stem Cells. 2008; 26:1056–1064. [PubMed: 18218819]

Tai K, Pelled G, Sheyn D, Bershteyn A, Han L, Kallai I, Zilberman Y, Ortiz C, Gazit D. Nanobiomechanics of repair bone regenerated by genetically modified mesenchymal stem cells. Tissue Eng Part A. 2008; 14:1709–1720. [PubMed: 18620480]

Turgeman G, Pittman DD, Muller R, Kurkalli BG, Zhou S, Pelled G, Peyser A, Zilberman Y, Moutsatsos IK, Gazit D. Engineered human mesenchymal stem cells: A novel platform for skeletal cell mediated gene therapy. J Gene Med. 2001; 3:240–251. [PubMed: 11437329]

van Lenthe GH, Voide R, Boyd SK, Muller R. Tissue modulus calculated from beam theory is biased by bone size and geometry: Implications for the use of three-point bending tests to determine bone tissue modulus. Bone. 2008; 43:717–723. [PubMed: 18639658]

van Rietbergen B, Weinans H, Huiskes R, Odgaard A. A new method to determine trabecular bone elastic properties and loading using micromechanical finite-element models. J Biomech. 1995; 28:69–81. [PubMed: 7852443]

Zilberman Y, Kallai I, Gafni Y, Pelled G, Kossodo S, Yared W, Gazit D. Fluorescence molecular tomography enables in vivo visualization and quantification of nonunion fracture repair induced by genetically engineered mesenchymal stem cells. J Orthop Res. 2008; 26:522–530. [PubMed: 17985393]

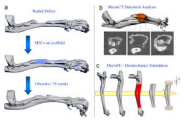

Figure 1.

The experimental design of the study. a) A 2.5-mm nonunion defect was created in the radius bone of each mouse. 2×10^6 genetically engineered MSCs were loaded onto a collagen sponge and implanted into the bone defect. The contralateral limb of the same mice, which were not subjected to surgery, was used as controls. 10 and 35 weeks after implantation, the mouse forelimbs (including the ulna and radius) were harvested; b) The forelimbs were scanned using a Micro-CT Scanner and the structural indices of the bone in the central 2 mm of the defect were determined; c) The micro-FE models were created for the middle 8 mm of the radius, including the ulna. The distal part of the model was fixed, and the proximal part underwent an axial displacement, resulting in 1% overall strain.

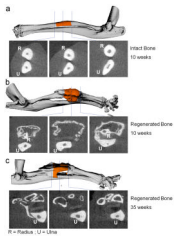

Figure 2.
Three-dimensional micro-CT imaging of intact and regenerated radial bones, 10 and 35 weeks after transplantation of genetically engineered MSCs. Cross sections obtained at different locations within the limbs are shown as 2D images. A quantitative analysis of bone formation in the central 2 mm of the radial defect and intact bone (highlighted in orange color) was performed (shown in figure 3).

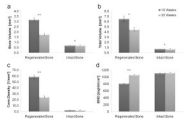

Figure 3.
Micro-CT analysis of the microarchitecture of regenerated and intact radial bones, at 10 and 35 weeks after implantation of genetically engineered MSCs. A quantitative analysis of the central 2 mm of the bones was performed. Statistical significant differences (two-tailed homoscedastic student's t-tests) between the 10 and 35 weeks groups are marked: *$p < 0.05$; **$p < 0.001$.

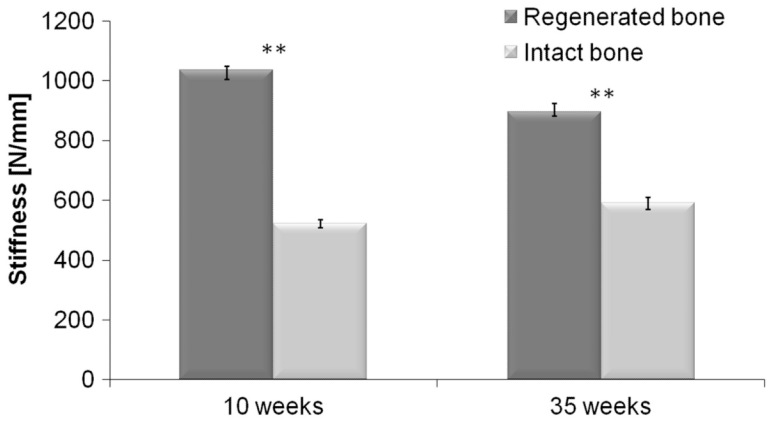

Figure 4.

Micro-FE analysis of regenerated and intact radial bones, at 10 and 35 weeks after implantation of genetically engineered MSCs, using a tissue modulus of 13.4 GPa. Statistical significant differences (two tailed homoscedastic student's t-tests) between the regenerated and intact bone groups are marked: *$p < 0.05$; **$p < 0.001$.

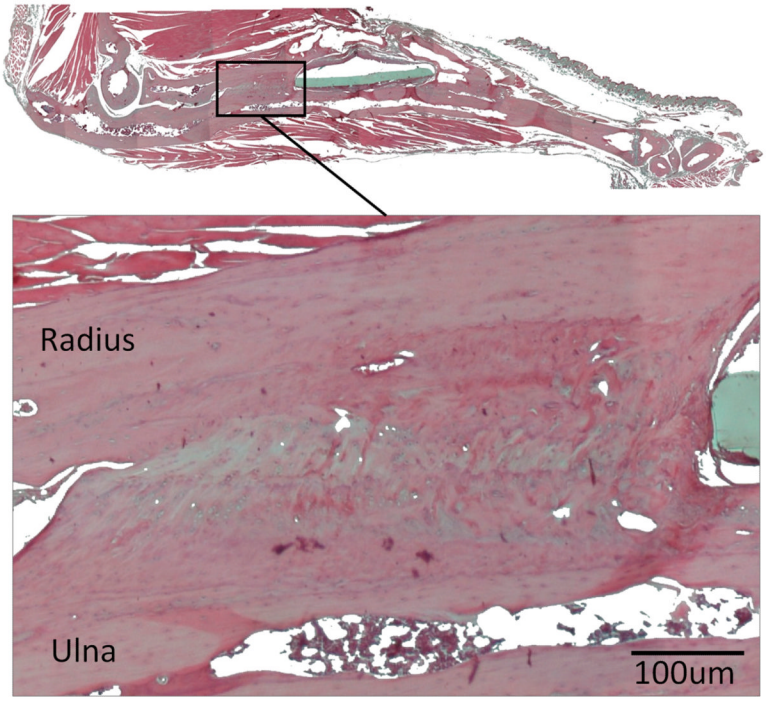

Figure 5.
Photomicrograph of hematoxylin and eosin (H&E) stained, decalcified, paraffin-embedded, 5-μm tissue section of a regenerated bone, 35 weeks after implantation of genetically engineered MSCs. The histology showed high degree of fusion between the radius and the ulna that could be the cause for the substantial increase in stiffness of the regenerated bones.

Table 1

Summary comparison of the structural and biomechanical properties of regenerated and intact bones. All values are mean values shown with ± standard error (n = 11).

Structural Index	Regenerated Bone		Intact Bone	
	10 weeks	35 weeks	10 weeks	35 weeks
Total Volume (TV, mm^3)	6.51 ± 0.56	4.53 ± 0.39	0.72 ± 0.01	0.77 ± 0.02
Bone Volume (BV, mm^3)	3.17 ± 0.21	1.79 ± 0.11	0.68 ± 0.01	0.72 ± 0.02
Bone Volume Density (BV/TV)	0.51 ± 0.04	0.42 ± 0.03	0.95 ± 0.00	0.94 ± 0.01
Connectivity Density ($1/mm^3$)	58.59 ± 3.51	24.93 ± 1.91	2.13 ± 0.42	2.28 ± 0.58
Bone Thickness (B.Th, mm)	0.14 ± 0.00	0.12 ± 0.01	0.29 ± 0.00	0.29 ± 0.00
Bone Separation (B.Sp, mm)	0.37 ± 0.05	0.34 ± 0.02	0.09 ± 0.00	0.12 ± 0.01
Bone Mineral Density (mg HA/cm^3)	809.15 ± 11.25	1069.58 ± 6.70	1109.08 ± 11.58	1129.98 ± 10.21
Degree of Anisotropy (DA)	1.28 ± 0.02	1.75 ± 0.05	8.31 ± 0.34	8.51 ± 0.29
Axial Stiffness (N/mm)	1035.53 ± 13.44	895.88 ± 29.83	522.76 ± 13.97	590.54 ± 19.93

Table 2

Summary of p-values (two tailed homoscedastic student's t-tests). Statistical significant differences are marked (*p < 0.05; **p < 0.001).

Structural Index	10 vs. 35 weeks		Regenerated vs. Intact Bone	
	Regenerated Bone	Intact Bone	10 weeks	35 weeks
Total Volume (TV, mm^3)	9.43E-03 *	2.17E-02 *	2.08E-09 **	7.06E-09 **
Bone Volume (BV, mm^3)	7.30E-06 **	2.62E-02 *	1.17E-10 **	2.98E-09 **
Bone Volume Density (BV/TV)	5.44E-02 *	9.86E-02	9.11E-11 **	3.12E-13 **
Connectivity Density ($1/mm^3$)	5.14E-08 **	8.38E-01	7.48E-13 **	3.52E-10 **
Bone Thickness (B.Th, mm)	3.25E-02 *	6.57E-01	6.76E-18 **	2.30E-16 **
Bone Separation (B.Sp, mm)	6.04E-01	1.92E-02 *	5.72E-06 **	3.14E-08 **
Bone Mineral Density (mg HA/cm^3)	1.20E-14 **	1.91E-01	4.41E-14 **	7.76E-05 **
Degree of Anisotropy (DA)	9.27E-08 **	6.63E-01	5.59E-15 **	6.24E-16 **
Axial Stiffness (N/mm)	3.75E-04 **	1.14E-02 *	4.91E-17 **	4.42E-08 **